Partitioning of Spherical Solutes into Sponge-Type Materials

Partition coefficients are computed for hard spherical solutes in equilibrium with sponge-type matrices containing randomly-placed spherical cavities or pores using grand canonical Monte Carlo simulation. The random pore model is representative of a variety of disordered porous solids including porous glasses and some polymeric materials. The algorithm used brings additional realism to the problem by rigorously distinguishing between accessible and inaccessible pore space. The simulation results display significant concentration effects which are often observed experimentally and are compared to data obtained by Brannon and Anderson (1982) for the partitioning of bovine serum albumin into controlled-pore glass.

Lisa A. Fanti
Eduardo D. Glandt
Department of Chemical Engineering
University of Pennsylvania
Philadelphia, PA 19104

Introduction

Size exclusion chromatographs and drug delivery devices are examples of systems driven by the equilibrium partitioning of a solute between a bulk fluid phase and a porous solid matrix (Yau, 1971; Langer and Folkman, 1976). The desire to control and fine-tune such processes in order to separate and manipulate highly specialized polymer and biological macromolecules has prompted a significant interest in the underlying physics of the partitioning process. The degree of partitioning is usually characterized by the partition coefficient K, which is the ratio of the solute concentration within the pore phase of the solid to its concentration in the bulk phase in equilibrium with it. The partition coefficient is, of course, very dependent upon solute-solute and solute-matrix interactions, along with the often highly complex microstructure of the porous solid material. Experimental evidence has also suggested a less obvious, but significant, dependence on the concentration of solute in the bulk phase. The fundamental modeling of this phenomenon can provide a valuable framework for the systematic manipulation of solvents and porous materials to attain very specialized results.

One class of structures often encountered is that of sponge-like matrices. These include a variety of porous-glass materials, such as Vycor (Dow Corning), which are commonly used because they can be prepared with consistency and are easily regenerated. They are usually made of a borosilicate (or similar) glass melt, which is cooled below its demixing temperature to cause spinodal decomposition into a silicate-rich and a borate-rich phase. The pore space is then formed by leaching the latter. The result is a homogeneous, sponge-like microstructure, usually containing a mean pore size in the submicron range. Figure 1a displays an electron micrograph of such a material (Wiltzius et al., 1987). Several polymeric materials, such as the membrane shown in Figure 1b (Castro, 1981), are also characterized by a sponge-like microstructure. This particular sample was manufactured using a thermal sol-gel phase inversion process. This involves preparing a polymer solution containing a latent solvent (effective only at elevated temperatures) that, upon cooling, becomes immiscible and *inverts* to a sol-containing spherical micelles of solvent. The suspension is then permitted to gel, and the latent solvent (often a solid at room temperature) is extracted using a second solvent. This technique preserves the spherical geometry of the pores, which is present in the sol state and is widely applicable to a variety of polymers which are only soluble at elevated temperatures (Kesting, 1985).

Due to the high complexity of the partitioning process, modeling achievements in this area have been somewhat limited. A significant amount of work exists on the partitioning of spherical solutes into geometrically ideal pores such as cylinders, spherical cavities, and infinite slits, following the seminal work of Giddings et al. (1968). Some of the methods used include virial expansions (Glandt, 1980, 1981; Anderson and Brannon, 1981; Smith and Deen, 1980, 1983; Mitchell and Deen, 1984; Post and Glandt, 1985), Monte Carlo simulations (MacElroy *and* Suh, 1986, 1987), integral equation theories (Zhou and Stell, 1989a,b), and density functional theories (Post, 1988). The effects of solute size, solute concentration and electrostatic interactions were readily observed and qualitatively confirmed many of the experimental observations. Other efforts have been concerned with the partitioning of highly dilute flexible chain

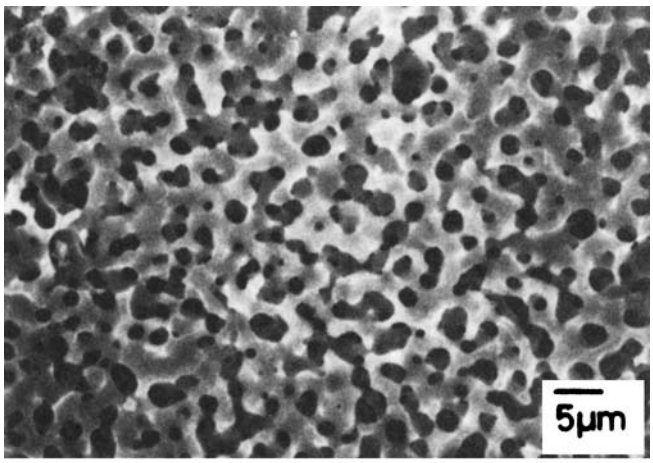

A

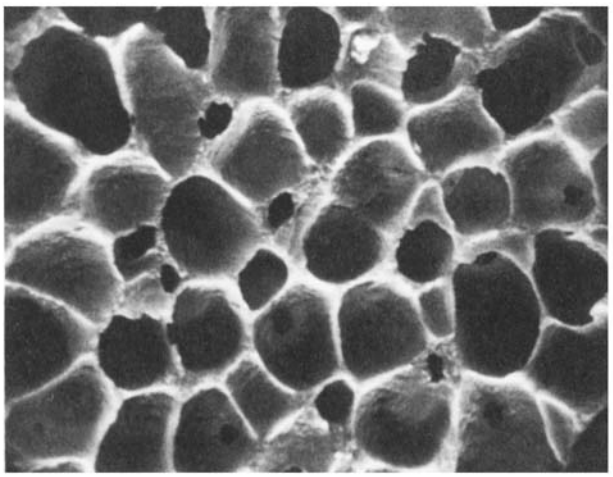

B

a. *Porous glass prepared by acid leaching*
b. *Polymer membrane prepared by thermal phase inversion*

Figure 1. Sponge-like materials.

molecules in regular pores (Casassa, 1967; Davidson et al., 1987). Recently, Limbach et al. (1989) studied the partitioning of rigid nonspherical molecules in pores of various geometries, again in the limit of infinite dilution. They also considered the partitioning of spherical solutes into regular structures designed to mimic the geometry of random media: corrugated slits and regular packings of spheres and of cylinders.

A regular geometry always implies an idealization that oversimplifies the matters of connectivity and accessibility of the pore space and that restricts the applicability of the above results. Other works introduced the effect of the disordered nature of the porous solid by studying model structures composed of random fibers (Ogston, 1958), randomly oriented planes (Giddings et al., 1968) and randomly overlapping spheres (Rikvold and Stell, 1985). The above efforts, however, have been limited to the Henry's law regime, in which the solute is infinitely dilute. They do not consider or predict the concentration effects which are often experimentally observed.

More recently, Fanti and Glandt (1989a,b) have used a statistical mechanical approach (Monte Carlo simulations and density functional theory) to determine partition coefficients for compact macromolecules, regarded as hard spherical solutes, at moderate to high concentrations in equilibrium with fibrous matrices. Similarly, the present work addresses the partitioning of concentrated spherical solutes into *sponge-like* matrices using Monte Carlo simulation. The following section describes the model used and the parameters necessary to characterize it. It also contains an approximate result for partitioning in the limit of high dilution of solute particles, i.e., the Henry's law constant. The next section addresses the issue of the accessibility of the pore space and outlines the computation of the "filtration percolation" threshold for this model. Following this, the algorithm used to compute partition coefficients from grand canonical Monte Carlo simulations is summarized. A derivation of the osmotic pressure equation is presented next, along with an alternate method for computing the partition coefficient from this pressure. In the final section, results for the random pore model are discussed and compared to experimental data for the partitioning of bovine serum albumin into controlled-pore glass.

General Definitions

Consider a bulk solution of spherical or quasispherical particles in equilibrium with a sponge-like matrix. The model matrix considered here consists of a solid phase which contains spherical cavities or pores of diameter D. At moderate to high porosities, the cavities overlap extensively to form an interconnected network. The resulting structure is statistically homogeneous and isotropic, and is assumed to be rigid, i.e., *it is not affected by the introduction of the solute.* The pores are distributed randomly with number density ρ_c. A dimensionless number density of the cavities can be defined as

$$\eta_c = \frac{\pi}{6} \rho_c D^3 \tag{1}$$

This quantity is trivially related to the total porosity ψ of the structure by

$$\psi = 1 - \exp\{-\eta_c\} \tag{2}$$

Figure 2 displays a schematic representation of the model.

The interactions used in this work are the simplest possible: steric exclusions between solutes and between each solute and the matrix walls. If r denotes the center-to-center distance

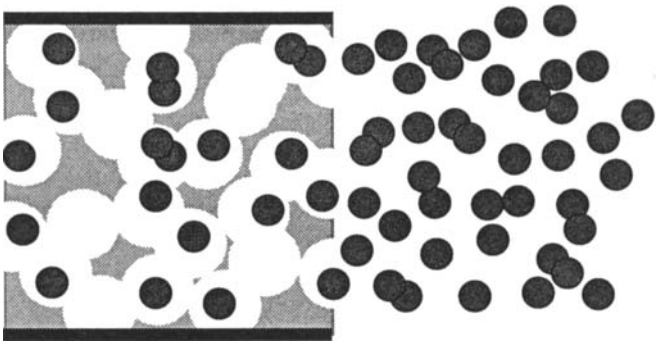

Figure 2. Random pore model.
The presence of the matrix establishes a concentration difference between the bulk phase and the pore space.

between two particles, the solute-solute pair potential energy is

$$u_{ss}(r) = \infty \quad r < d$$
$$= 0 \quad r > d \tag{3a}$$

where d is the particle diameter. Similarly, the potential energy of interaction of a particle within an individual cavity can be given by

$$u_{cs}(t) = \infty \quad t < d/2$$
$$= 0 \quad t > d/2 \tag{3b}$$

where t denotes the distance between the particle and the point of closest approach to the periphery of the pore. Note that the term *periphery* is taken to denote the entire spherical surface of the cavity, including both those portions that correspond to solid wall and those that lie inside other pores. The above relations are only well defined when $t \leq D/2$.

The interaction energies of Eq. 3b are not pairwise-additive. This would prohibit configurations in which a solute is closer than $d/2$ to the edge of any cavity, whereas such configurations are actually possible because the pores overlap. For example, although the solute particle in Figure 3 lies outside the periphery of the left cavity, the interaction energy between this solute and the matrix is zero because the particle lies inside the right pore. The solute-matrix configurational energy for N particles and M pores is not obtained by adding the u_{cs}, but can be computed as

$$U_{cs} = kT \sum_{j=1}^{N} \ln\left[1 - \prod_{i=1}^{M} [1 - \exp(-u_{ij}/kT)]\right] \tag{4}$$

This expression yields $U_{cs} = 0$ as long as every solute particle is *fully* inside at least one pore, i.e., $t_{\vec{y}} > d/2$. Equation 4 is actually an approximation because a particle need not overlap with the solid even if is not fully inside *any* pore. For the matrix shown in Figure 3, the black regions are those which are neglected in this approximation. It is important to note that all of our calculations invoke the McMillan-Mayer formalism (1945), i.e., the interactions of Eqs. 3 are potentials of mean force: they incorporate all effects due to the solvent in which the solute is suspended.

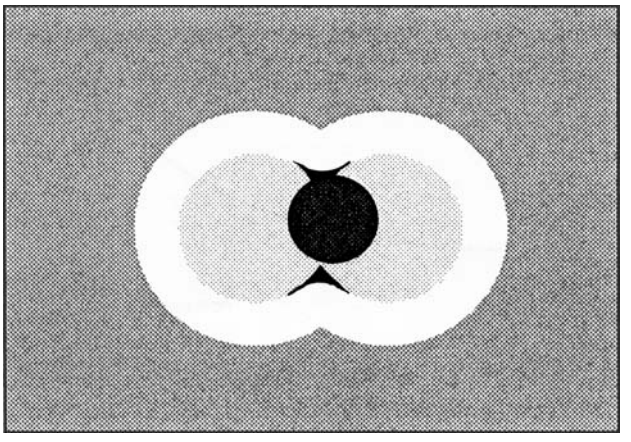

Figure 3. Possible configurations of a solute within the random pore model.

The lightly shaded regions are energetically accessible to the center of a solute according to the interactions of Eq. 3. The blackened regions are those which should be included, but are neglected in this approximation.

The sponge-like matrix is assumed to be in equilibrium with a bulk solution or dispersion of particles, of number concentration ρ_b. This concentration is expressed in dimensionless form by the bulk particle volume fraction

$$\eta_b = \frac{\pi}{6} \rho_b d^3 \tag{5}$$

It is also appropriate to define a dimensionless relative solute size $\lambda = d/D$. For a given porosity ψ, relative solute size λ, and bulk-phase concentration η_b, the particle concentration will vary from point to point within the matrix. The quantity of interest is ρ_s, the average solute concentration in the matrix. Note that ρ_s designates the concentration based upon the pore volume only and not on the entire volume of the system. Equivalently, ρ_s may also be regarded as the average concentration at some fixed point *within the pore space*, taken over the ensemble of all random configurations of the pores. The partition coefficient, which expresses ρ_s in dimensionless form, is defined as

$$K = \frac{\rho_s}{\rho_b} \tag{6}$$

At high dilution, particle-particle interactions are negligible, and increasing the bulk concentration will result in a proportional increase in concentration within the porous phase. In this case, which is the Henry's law regime

$$\rho_s = H\rho_b \tag{7}$$

where $H = \lim_{\rho_b \to 0} K$ is the Henry's law constant. For a model like the one considered here, in which the only energetic interactions are steric exclusions, the Henry's law constant is simply given by the fraction of volume available to a particle center within the porous matrix. The available volume is very closely approximated by that of a set of overlapping spheres, each of diameter $D - d$, with the same coordinates as the cavities in the porous matrix. As discussed above, this estimate slightly underestimates the Henry's constant because it does not account for certain portions of the pore space which are made available to the solutes by pore overlap (see Figure 3). It is straightforward to show that, within this approximation, the fractional free volume is given by

$$H = \frac{1 - \exp[-\eta_c(1 - \lambda)^3]}{1 - \exp[-\eta_c]} \tag{8}$$

At higher concentrations, particle-particle interactions are expected to cause marked deviations from Henry's law.

Pore Accessibility: Filtration Percolation

In studying partitioning into disordered porous materials it is necessary to consider the extent to which a solute can access the pore space. Figure 4a shows a solid matrix of low porosity containing a hard spherical solute. Those portions of the pore space which could potentially be occupied by the center of this particle are indicated in black. These regions consist of localized "islands" which are actually inaccessible, with the exception of

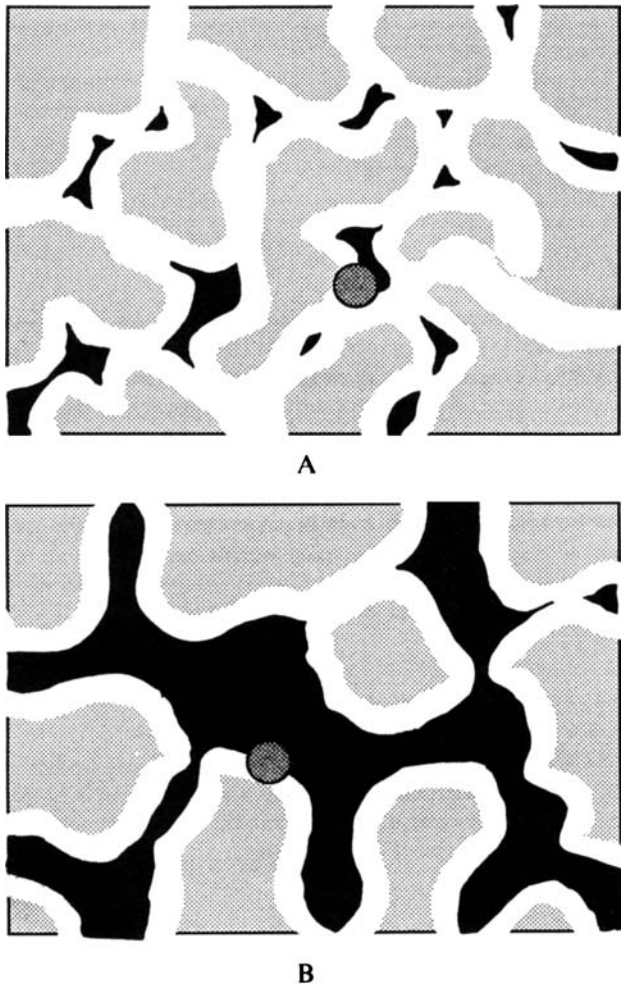

Figure 4. Filtration percolation in porous materials.

Structure a is not percolated and therefore does not permit the macroscopic transport of solutes.
Structure b, which is more porous, is percolated and does allow solute transport.

some limited sections at the boundary of the material. In contrast, Figure 4b shows a solute of the same size contained within a similar matrix of a higher porosity. In this case, most of the available regions are not isolated, but are interconnected and span the structure, indicating that macroscopic transport within the solid is possible.

Percolation theory (Stauffer, 1985) provides a formalism for the calculation of the extent to which solutes of different sizes can penetrate a porous material. For given particle and pore sizes, we define the critical porosity at which the *accessible* pore space spans the solid in all directions as the *filtration percolation threshold*. The threshold for particles of finite size can be calculated from the percolation threshold for particles of zero size, which is known. The porosity ψ_c at which a random assembly of overlapping pores percolates has been obtained by several methods including virial expansions (Haan and Zwanzig, 1977), integral equation theories (Chiew and Glandt, 1983; Chiew et al., 1985; Chiew and Stell, 1989), and Monte Carlo simulations (Pike and Seager, 1974; Safran et al., 1985). The simulations consistently yield a value of $\psi_c = 0.29$. The percolation threshold for solutes of finite size is higher than 0.29, because larger particles are unable to pass through narrower necks within a matrix of this porosity. The percolation problem for particles of size d in a matrix of pores of diameter D is equivalent to that of a particle of zero size through a matrix of pores of diameter D' where

$$D' = [D^2 - d^2]^{1/2} \tag{9}$$

Figure 5 shows the filtration percolation threshold ψ_c as a function of the relative solute size λ, as obtained using Eq. 9. Systems falling within the upper portion of this phase diagram are percolated and permit macroscopic transport of solutes, whereas those within the lower region do not.

Monte Carlo Simulations

Partition coefficients were computed directly by Monte Carlo simulation for a variety of solute concentrations, relative solute sizes, and porosities using a straightforward algorithm in the grand-canonical ensemble (Adams, 1974 and 1975). In this ensemble, the independent variables are volume and chemical potential, and the computed results are the pressure and number concentration of particles. The simulations involved fixing the bulk concentration and porosity, randomly distributing an arrangement of pores, and then eliminating those pores which were not accessible. Finally, solute particles were added, moved and removed until an equilibrium partition coefficient was obtained. The simulations performed here employed periodic boundary conditions. A very efficient algorithm was developed for detecting which pores were percolated or accessible within such systems; this method is outlined in detail elsewhere (Fanti, 1989). The remainder of the simulation procedure was a natural extension of a typical algorithm in the grand canonical ensemble. The following sequential steps were performed:

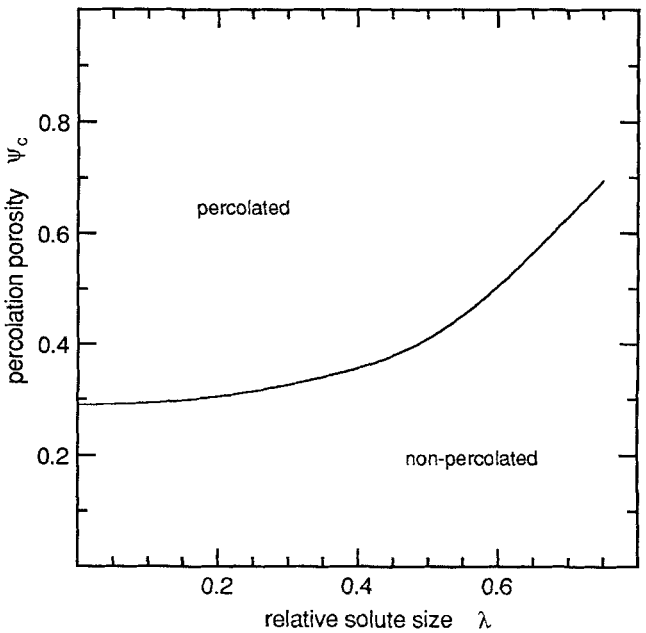

Figure 5. Filtration percolation thresholds for the random pore model.

Systems falling within the upper region of the phase diagram are percolated, while those falling within the lower region are not.

Step 1. Insert a particle into the matrix. The insertion was accepted, if there was no overlap with either the solid matrix or another particle, according to the probability ratio

$$\frac{P_{\text{new}}}{P_{\text{old}}} = \frac{a^*}{N+1} \tag{10}$$

Step 2. Displace a randomly-chosen particle within the matrix. The move was accepted if there was no overlap with either the solid matrix or another particle.

Step 3. Remove a randomly chosen particle from the matrix. The removal was accepted according to the probability ratio

$$\frac{P_{\text{new}}}{P_{\text{old}}} = \frac{N}{a^*} \tag{11}$$

In Eqs. 10 and 11, $a^* = \rho_b \phi_b V$ is the reduced activity of the solute particles, where ϕ_b is the activity (or fugacity) coefficient, which was computed prior to the simulation from the Carnahan-Starling relation for hard spheres (1969)

$$\ln \phi_b = \frac{8\eta_b - 9\eta_b^2 + 3\eta_b^3}{(1-\eta_b)^3} \tag{12}$$

This relation is highly accurate for the range of concentrations considered here. The above algorithm is applicable without any modification to any random medium in which the interactions are solely steric exclusions. Its extension to more realistic (such as adsorptive) interactions is simple and straightforward.

Simulations were carried out for matrices with porosities of $\psi = 0.35, 0.45$, and 0.55, relative solute sizes of 1/4, 1/3, and 1/2, and for bulk concentrations $\eta_b = 0.05, 0.10, 0.15, 0.20$, and 0.25. The number of pores in the system was between 15 and 100 for all runs. At the highest porosity and high particle concentrations, only 15 cavities were used to prevent the number of particles from exceeding 200. At the lowest porosity and low particle concentrations, 100 pores were used to keep the particle number high enough to obtain good statistics. Each simulation was allowed to relax for 50,000 cycles, at which point the statistics were shown to be uncorrelated from the initial configuration, in accordance with the method of Kolafa (1986). There were a minimum of 5,000 cycles per particle performed, which was sufficient to produce a statistically invariant partition coefficient.

Table 1. Partition Coefficients As Determined Directly from the Monte Carlo Simulation and Indirectly from the Pressure Equation for a Porosity of $\psi = 0.35$

λ	η_b	$K_{\text{simulation}}$	K_{pressure}
0.25	0.00	0.475	0.475
0.25	0.05	0.527 ± 6	0.531
0.25	0.10	0.583 ± 6	0.588
0.25	0.15	0.631 ± 4	0.643
0.25	0.20	0.678 ± 8	0.695
0.25	0.25	0.718 ± 8	0.743
0.33	0.00	0.342	0.342
0.33	0.05	0.412 ± 6	0.403
0.33	0.10	0.477 ± 4	0.498
0.33	0.15	0.540 ± 5	0.570
0.33	0.20	0.600 ± 5	0.626
0.33	0.25	0.639 ± 1	0.681

Table 2. Partition Coefficients As Determined Directly from the Monte Carlo Simulation and Indirectly from the Pressure Equation for a Porosity of $\psi = 0.45$

λ	η_b	$K_{\text{simulation}}$	K_{pressure}
0.25	0.00	0.495	0.495
0.25	0.05	0.548 ± 1	0.558
0.25	0.10	0.605 ± 1	0.622
0.25	0.15	0.653 ± 1	0.671
0.25	0.20	0.695 ± 8	0.721
0.25	0.25	0.736 ± 8	0.772
0.33	0.00	0.361	0.361
0.33	0.05	0.428 ± 3	0.441
0.33	0.10	0.493 ± 3	0.517
0.33	0.15	0.556 ± 2	0.582
0.33	0.20	0.615 ± 2	0.646
0.33	0.25	0.664 ± 3	0.706
0.50	0.00	0.160	0.160
0.50	0.05	0.226 ± 4	0.277
0.50	0.10	0.311 ± 2	0.328
0.50	0.15	0.408 ± 2	0.462
0.50	0.20	0.488 ± 1	0.595
0.50	0.25	0.523 ± 2	0.693

The partition coefficients obtained from the simulations at the three porosities are presented in Tables 1–3 and in Figures 6a–c. Each of these values is an average over five or more independent configurations of pores. The primary source of the error reported is from variations between matrix configurations and not from the individual simulations.

Thermodynamic Properties

To compute thermodynamic properties within porous media, it is useful to obtain statistical distribution functions such as the average concentration profile $\rho_{ws}(t)$ from a pore wall. This distribution is the conceptual result of averaging the local concentration at a distance t from a solid pore wall over the positions of the remaining pores. It can be expressed in reduced form as $g_{ws}(t)$,

Table 3. Partition Coefficients As Determined Directly from the Monte Carlo Simulation and Indirectly from the Pressure Equation for a Porosity of $\psi = 0.55$

λ	η_b	$K_{\text{simulation}}$	K_{pressure}
0.25	0.00	0.520	0.520
0.25	0.05	0.579 ± 3	0.585
0.25	0.10	0.633 ± 3	0.646
0.25	0.15	0.680 ± 3	0.702
0.25	0.20	0.722 ± 2	0.752
0.25	0.25	0.755 ± 9	0.799
0.33	0.00	0.383	0.383
0.33	0.05	0.451 ± 1	0.466
0.33	0.10	0.519 ± 1	0.546
0.33	0.15	0.577 ± 6	0.612
0.33	0.20	0.634 ± 6	0.677
0.33	0.25	0.680 ± 4	0.734
0.50	0.00	0.173	0.173
0.50	0.05	0.232 ± 3	0.240
0.50	0.10	0.319 ± 2	0.344
0.50	0.15	0.419 ± 2	0.479
0.50	0.20	0.498 ± 3	0.612
0.50	0.25	0.536 ± 3	0.712

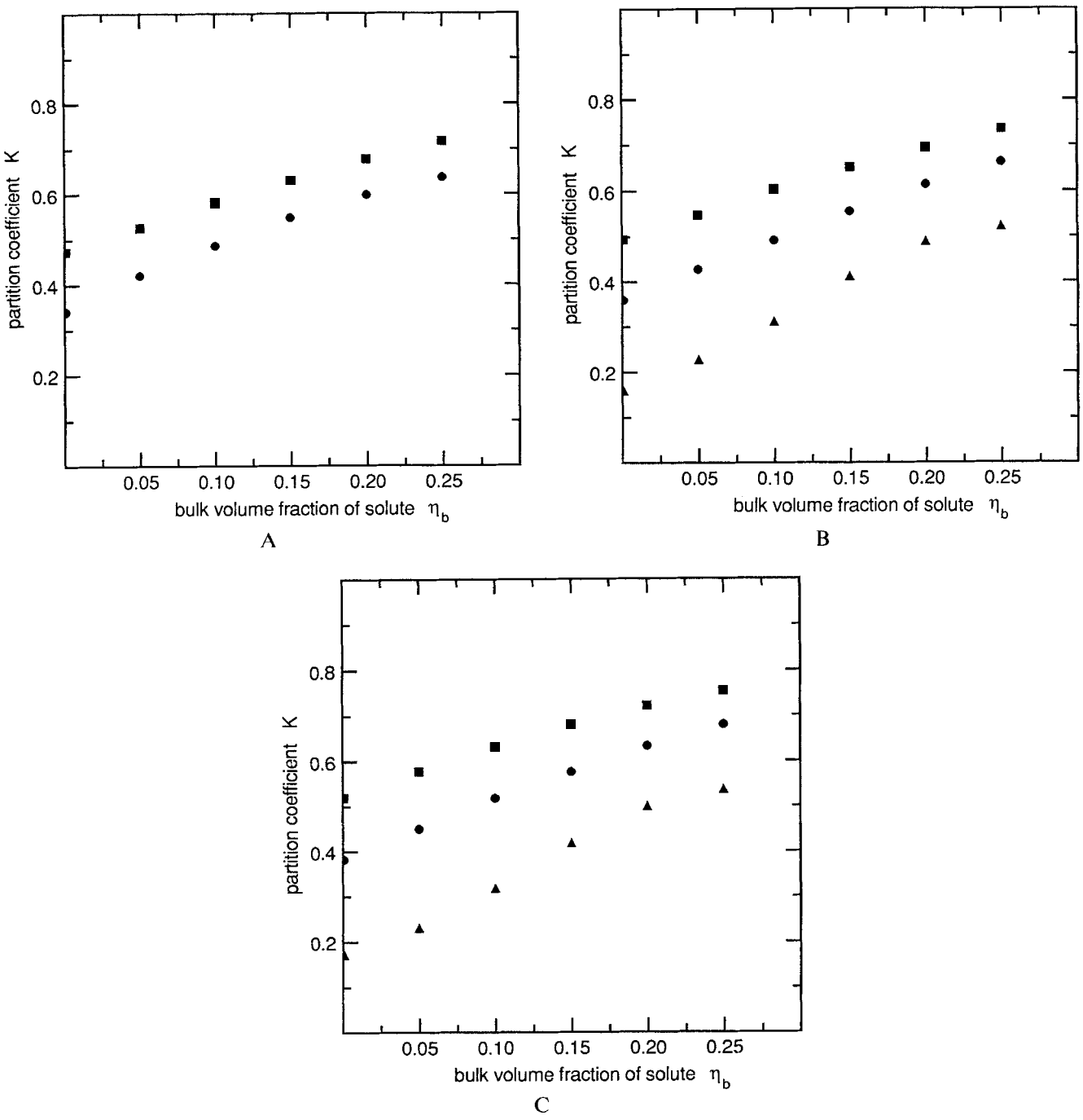

a. *For a porosity of* $\psi = 0.35$, $\lambda = 1/4$ *(squares), and* $\lambda = 1/3$ *(circles)*
b. *For a porosity of* $\psi = 0.45$, $\lambda = 1/4$ *(squares), and* $\lambda = 1/3$ *(circles), and* $\lambda = 1/2$*(triangles)*
c. *For a porosity of* $\psi = 0.55$, $\lambda = 1/4$ *(squares), and* $\lambda = 1/3$ *(circles), and* $\lambda = 1/2$ *(triangles)*

Figure 6. Partition coefficients as a function of bulk concentration η_b obtained directly from the Monte Carlo simulations.

the wall-solute pair correlation function, where $\rho_{ws}(t) = \rho_s g_{ws}(t)$. The correlation $g_{ws}(t)$ was normalized here so that $g_{ws}(t) = 1$ (for $t < D$) if the solute diameter is zero. Similarly, the solute-solute pair correlation function $g_{ss}(r)$ was defined such that $\rho_s \psi g_{ss}(r)$ is the probability density of finding a particle at a distance r from another particle within the matrix. At large separations within the matrix, $g_{ss}(r) \rightarrow 1$.

One thermodynamic property of interest is the osmotic pressure Π_m as a function of bulk concentration, because it provides an alternative method for the computation of the partition coefficient. We define Π_m as the sum of the stresses resulting from both solute-solute and matrix-solute interactions. This definition does not include the stresses carried by the solid matrix due to the presence of the solute particles and will be different from

that of the bulk solution in equilibrium with it. When the stresses carried by the solid are added to Π_m, the sum must be equal to the bulk osmotic pressure Π_b, so that mechanical equilibrium is indeed satisfied. For hard spheres, Π_b is accurately computed using the Carnahan-Starling equation of state (1969).

An expression for Π_m can be derived by passing an arbitrary plane through the medium and computing the average configurational force across the plane. The position vectors r_1 and r_2 represent the $\{x, y, z\}$ coordinates of points in the upper and lower half spaces which are divided by the arbitrary plane and define a "line of action" which intersects the $z = 0$ plane. The length of the line of action is $t = |r_2 - r_1|$. The total force is obtained by integrating r_1 and r_2 over their respective half-spaces. For the random pore model, this force is given by

$$F = -\psi^2 \int \rho_s^2 s g_{ss}(t)\, u'_{ss}(t) \cos\theta \, dr_1 \, dr_2 - 2(1-\psi) \int \rho_s \rho_p(t)\, g_{ws}(t)\, u'_{cs}(t) \cos\theta \, dr_1 \, dr_2 \quad (13)$$

The second term in the above expression represents the interactions between solute particles and the solid. For convenience, the locations of the pores are described by the distances from their peripheries, and not their centers, to an arbitary origin. In Eq. 13, $\rho_p(t)$ is the number density of such periphery points located a distance t away from the origin. Periphery points are located by projecting a straight line from the arbitrary origin through the center and to the *concave* periphery of each pore. All such points are included, regardless of whether or not they are located on solid walls. Figure 7 shows a typical matrix and the points included in ρ_p. Note that pores which contain the arbitrary origin have *two* periphery points. For a random pore matrix, the density of these points is not uniform, but is given by $\rho_p(t) = \rho_c [1 - D/t + D^2/4t^2]$. This result is derived in the Appendix.

The line of action intersects the reference plane at coordinates (x, y) and at a polar angle θ and azimuthal angle ϕ. It is convenient to adopt a coordinate transformation

$$\begin{aligned} x_1 &= x + t' \sin\theta \cos\phi \\ y_1 &= y + t' \sin\theta \sin\phi \\ z_1 &= t' \cos\theta \\ x_2 &= x - (t - t') \sin\theta \cos\phi \\ y_2 &= y - (t - t') \sin\theta \sin\phi \\ z_2 &= -(t - t') \cos\theta \end{aligned} \quad (14)$$

Here t' is that portion of t which falls within the upper half space. Restricting the integration to a unit area of the $z = 0$ plane gives an equation for the osmotic pressure

$$\frac{\Pi_m}{\psi \rho_s kT} = 1 + \frac{2\pi}{3} \psi \rho_s d^3 g_{ss}(d) + \frac{1-\psi}{\psi} \eta_c \left[\lambda^3 - 2\lambda^2 + \lambda\right] g_{ws}\left(\frac{d}{2}\right) \quad (15)$$

The equilibrium partition coefficient K can be computed from the osmotic pressure Π_m by constructing a thermodynamic path between solute in the bulk state and within the porous matrix. The chemical potential difference between a bulk solution of hard spheres at ρ_b and an ideal solute (i.e., noninteracting particles) at the same concentration is given very accurately by the

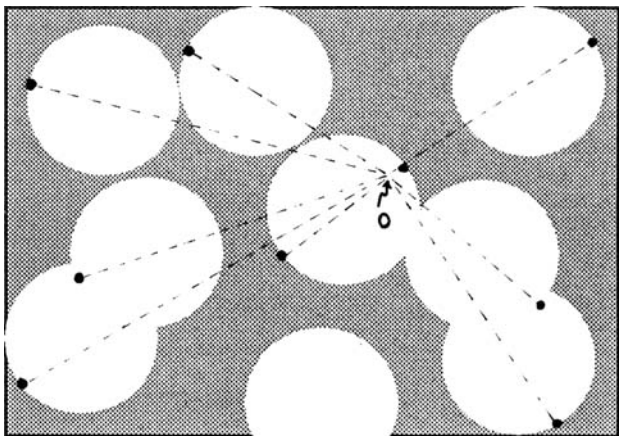

Figure 7. Location of periphery points in a matrix containing randomly distributed spherical pores.
All such points are included with ρ_p, regardless of whether or not they are located on a solid wall.

Carnahan-Starling (1969) relation

$$\frac{\Delta\mu}{RT} = -\frac{8\eta_b - 9\eta_b^2 + 3\eta_b^3}{(1-\eta_b)^3} \quad (16)$$

The corresponding difference between this ideal solute and an ideal solute at the matrix concentration ρ_s contains the (unknown) partition coefficient

$$\frac{\Delta\mu}{RT} = \ln\frac{\rho_s}{\rho_b} = \ln K \quad (17)$$

The difference between an ideal solute at the matrix concentration ρ_s and an ideal solute at the same concentration but *within the porous matrix* is given by Henry's law

$$\frac{\Delta\mu}{RT} = \ln\frac{1}{H} \quad (18)$$

Equation 18 applies for any value of the concentration ρ_s. The final step involves the computation of the chemical potential change from an ideal solute to a hard-sphere solute *within the porous matrix*. This requires the integration of the Gibbs-Duhem equation

$$V\, d\,\Pi_m = N\, d\mu \quad (19)$$

to yield

$$\frac{\Delta\mu}{RT} = \int_0^\rho (Z - Z_{\text{ideal}}) \frac{1}{\rho} d\rho + Z - Z_{\text{ideal}} \quad (20)$$

In the above expression, $Z = \Pi_m/\rho_s RT$, and Z_{ideal} is given by

$$Z_{\text{ideal}} = 1 + \frac{1-\psi}{H\psi} \eta_c [\lambda^3 - 2\lambda^2 + \lambda] \quad (21)$$

This quantity is not unity because such particles are still excluded by the pore walls.

In addition to the direct results presented in the previous sec-

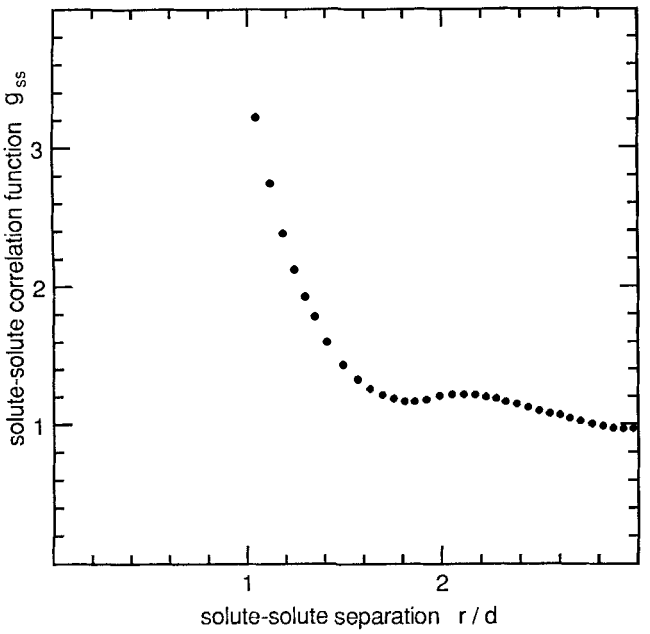

Figure 8a. Solute-solute pair correlation function.

tion, partition coefficients were also estimated using Eqs. 15–21 and data from the Monte Carlo simulations. The expressions for the number of pores η_c, the porosity ψ, and the Henry's law constant H presented in Eqs. 3, 4 and 8 include all pores and, therefore, are not correct if some of the pores are not accessible from the bulk phase. More appropriate values, which include the accessible regions only, were calculated within the simulations. When only accessible pores are considered, the expression for $\rho_p(t)$ derived in the Appendix is also no longer exact, but was utilized in Eq. 15 as an approximation. In addition $g_{ws}(t)$ was not rigorously computed, as it is very laborious to locate which portions of the cavity peripheries are actually hard walls. Instead, the cavity-solute pair distribution function, $g_{cs}(t)$, which describes the average concentration of solute a distance t from the *periphery* of a cavity, was substituted. Because $g_{cs}(d/2)$ includes solutes which are not truly in contact with a wall, it is expected to slightly underestimate $g_{ws}(d/2)$. Figures 8a and 8b display typical solute-solute and solute-cavity correlation functions obtained from the simulations. The osmotic pressures calculated within the above approximations are shown in Table 4, and the corresponding partition coefficients are presented in Tables 1–3.

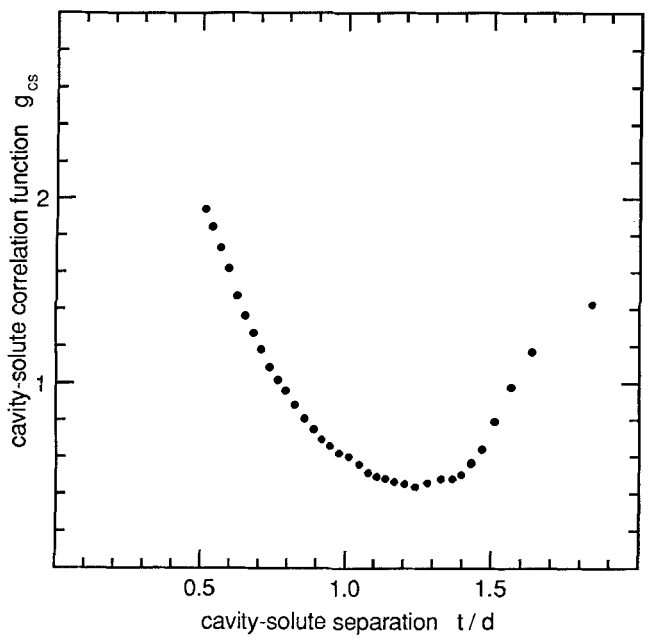

Figure 8b. Cavity-solute pair correlation function for ψ = 0.55, λ = 1/4, and η_b = 0.25.

Results and Discussion

Tables 1–3 and Figures 6a–c contain partition coefficients obtained from the Monte Carlo simulations for various porosities, relative solute sizes, and bulk concentrations. These tables also contain partition coefficients obtained by thermodynamic integration of the osmotic pressures shown in Table 4. The agreement is good in some cases and fair in others. The discrepancies are attributed primarily to the approximation of $g_{ws}(t)$ by $g_{cs}(t)$. As stated earlier, $g_{cs}(t)$ is expected to underestimate $g_{ws}(t)$, which results in the overestimation of the partition coefficient, as is observed in Tables 1–3. In all cases, the partition coefficients within random pore structures are seen to differ significantly from those predicted by Henry's law. This emphasizes the need to consider concentration effects in the modeling of partitioning. It is also apparent that K is a much stronger function of the relative solute size than that of the porosity for the range of parameters studied here.

Additional Monte Carlo simulations were performed using the above system to model experimental data for the partitioning of bovine serum albumin (BSA) into controlled-pore glass (CPG) (Brannon and Anderson, 1982). As discussed earlier, electron micrographs suggest that the random pore model is appropriate for describing the microstructure of porous glasses. In addition, the solute (BSA) is a compact and rigid ellipsoidal macromolecule which can be reasonably approximated by a hard sphere. These measurements were made using a mass-balance technique on porous glasses of two mean pore radii: CPG

Table 4. Osmotic Pressures $\Pi_m/\psi\rho_s kT$ As Obtained by Monte Carlo Simulation

λ	η_b	ψ = 0.35	ψ = 0.45	ψ = 0.55
0.25	0.00	1.240	1.206	1.181
0.25	0.05	1.404 ± 4	1.364 ± 3	1.342 ± 3
0.25	0.10	1.626 ± 4	1.586 ± 2	1.565 ± 4
0.25	0.15	1.919 ± 4	1.881 ± 5	1.854 ± 7
0.25	0.20	2.316 ± 3	2.267 ± 7	2.241 ± 2
0.25	0.25	2.82 ± 1	2.752 ± 8	2.72 ± 1
0.33	0.00	1.368	1.303	1.256
0.33	0.05	1.487 ± 4	1.419 ± 4	1.372 ± 4
0.33	0.10	1.666 ± 8	1.595 ± 4	1.556 ± 3
0.33	0.15	1.93 ± 1	1.877 ± 2	1.820 ± 3
0.33	0.20	2.31 ± 1	2.24 ± 1	2.17 ± 1
0.33	0.25	2.74 ± 1	2.69 ± 1	2.622 ± 5
0.50	0.00		1.609	1.473
0.50	0.05		1.618 ± 7	1.518 ± 7
0.50	0.10		1.656 ± 9	1.562 ± 8
0.50	0.15		1.73 ± 1	1.635 ± 8
0.50	0.20		1.83 ± 2	1.75 ± 1
0.50	0.25		1.99 ± 3	1.92 ± 1

Table 5. Physical Properties of the BSA/CPG System

	CPG 100	CPG 200
Pore Dia. by Mercury Intrusion (Å)	116	250
Pore Vol. per Mass of Bead (mL/g)	0.75	0.60
Dimensions of BSA (Å)		
Major Axis	140	
Minor Axis	40	
Mol. Wt. of BSA by		
Osmotic Pres. Meas.		5.9 ± 10^4

100 and CPG 200. In both cases, the glass was coated with glycophase-G to prevent adsorption of the solute. Some physical properties of the glasses and of BSA are summarized in Table 5. This information was sufficient to estimate all parameters required for the simulations, so that no empirical fitting was necessary.

An *equivalent* solute size for BSA was obtained by averaging over all possible orientations of an ellipsoid to obtain its mean projected diameter, a characteristic length first used by Giddings et al. (1968). The resulting value of $d = 69$ Å is consistent with that computed by Brannon and Anderson from the measured osmotic second virial coefficient and number-averaged molecular weight. Porosities were computed using the pore volume per mass of bead, along with the solid-glass density of 2.2 g/mL. The average cavity diameter D (and hence the relative solute size, λ) was calculated indirectly from the average pore size obtained by mercury intrusion. It is well known that the mean pore radii reported by this technique actually correspond to the limiting constrictions within the solid. Within a dispersion of random pores, it is easily shown that the average diameter of a constriction is $\pi D/4$. The appropriate cavity diameter for the simulations was computed accordingly. The experimental data, along with the Monte Carlo results, are displayed in Figure 9.

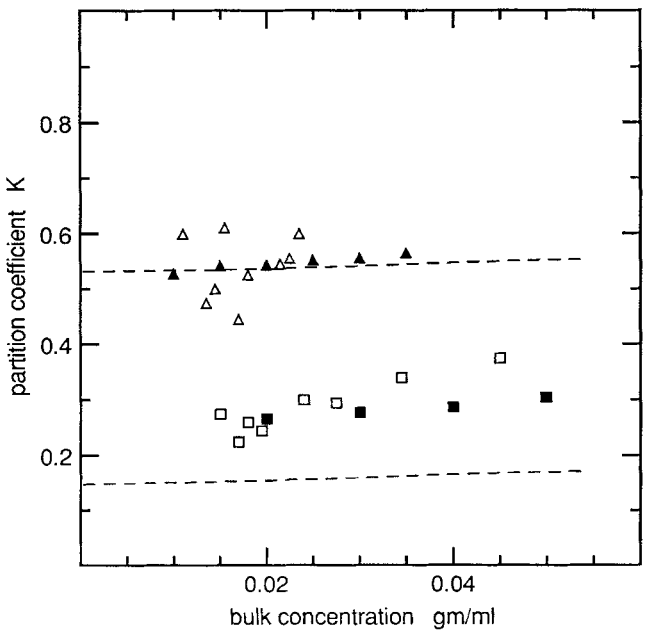

Figure 9. Partition coefficients for BSA in equilibrium with CPG.

The open squares and open triangles are the experimental data of Brannon and Anderson. The solid squares and solid triangles are the corresponding Monte Carlo results. Also shown as dashed lines are partition coefficients predicted using a cylindrical pore model.

The open triangles and open squares are the data for CPG 100 and CPG 200 respectively. The solid triangles and squares are the corresponding Monte Carlo results obtained using the random pore model. Also contained within this figure as dotted lines are the partition coefficients obtained using a cylindrical pore model (Glandt, 1981). Although the data are scattered, it is evident that the agreement between the experimental and simulation data is good in both cases. The cylindrical pore predictions are equally good for CPG 200, but somewhat poorer for CPG 100. As expected, in this case the more realistic random pore model yields better results than its geometrically ideal counterpart. The slight underestimation of the partition coefficient must be due to one or more of the assumptions involved in the calculations, such as the effective-diameter approximation to the ellipsoidal shape of the molecules.

Limbach et al. (1989) found that partitioning in regular models of granular materials could be successfully predicted using an equivalent cylindrical pore of the same *hydraulic* radius as the pores, i.e., using a characteristic pore size based on the specific area of the system. This useful empirical rule, however, breaks down in the case of random porosity. Since the interfacial area is not a monotonic function of the porosity but shows a maximum at intermediate values (Chiew and Glandt, 1984), the use of the hydraulic radius leads to unphysical results such as Henry's law constants that increase with increasing molecular size.

An extension of the calculations presented here to account for a distribution of pore sizes would be conceptually trivial, but laborious. Furthermore, there are some reasons to anticipate that the details of such distribution would have a minor effect. For example, the Henry's constant depends exclusively on the porosity and not on the pore sizes. Also, Chiew et al. (1985) found that, within the Percus-Yevick approximation, the percolation threshold of sponge-type structures can be expressed in terms of the porosity alone and is independent of other details of the pore size distribution.

Appendix: Average Density of Periphery Points

For $t > D/2$, the number of periphery points located at a distance t from an arbitrary origin is equal to the number of pore centers which are located at $t - D/2$. However, the *density* of such points ρ_p at t will be smaller than the density of pore centers ρ_c at $t - D/2$, because the differential volume of a spherical shell of radius t is larger than that of one with a radius $t - D/2$. The appropriate expression for ρ_p is therefore given by the (differential) number of cavity centers present at $t - D/2$ normalized by the (differential) volume at t

$$\rho_p(t) = \frac{\rho_c \, dV\,(t - D/2)}{dV(t)} \tag{A1}$$

$$= \frac{\rho_c \, 4\pi(t - D/2)^2 \, dt}{4\pi t^2 dt} \tag{A2}$$

Similarly, for $t < D/2$, ρ_p is given by the (differential) number of cavity centers present at $D/2 - t$, normalized by the (differen-

tial) volume at t.

$$\rho_p(t) = \frac{\rho_c\, dV\,(D/2 - t)}{dV(t)} \tag{A3}$$

$$= \frac{\rho_c\, 4\pi(D/2 - t)^2\, dt}{4\pi t^2 dt} \tag{A4}$$

In both cases, the final result is

$$\rho_p(t) = \rho_c\left[1 - \frac{D}{t} + \frac{1}{4}\left(\frac{D}{t}\right)^2\right] \tag{A5}$$

The number density of periphery points which are actually hard *walls* at a distance t from an arbitrary point is of course given by $(1 - \psi)\,\rho_p(t)$, since $(1 - \psi)$ is the solid volume fraction.

Acknowledgment

LAF is grateful to the AAUW for a predoctoral fellowship. The authors also acknowledge the allocation of supercomputer time by the John von Neumann Computer Center.

Notation

a^* = reduced activity
d = solute diameter
D = cavity diameter
g_{cs} = cavity-solute pair correlation function
g_{ss} = solute-solute pair correlation function
g_{ws} = wall-solute pair correlation function
H = Henry's law constant
K = partition coefficient
N = number of particles
P = probability of a configuration
r = solute-solute separation
R = ideal gas constant
t = cavity-solute separation
T = temperature
u_{cs} = cavity-solute interaction potential
u_{ss} = solute-solute interaction potential
U_{cs} = cavity-solute configurational energy
V = volume
Z = osmotic compressibility

Greek letters

ϕ_b = activity coefficient of bulk solution
η_b = reduced bulk concentration
η_c = reduced cavity density
λ = relative solute size
μ = chemical potential
Π_m = osmotic pressure within the matrix phase
Π_b = osmotic pressure in the bulk phase
ρ_b = number concentration of solute in the bulk phase
ρ_c = number density of cavities
ρ_p = number density of periphery points
ρ_s = number concentration of solute in the matrix phase
ρ_{ws} = concentration profile of solute in the vicinity of a wall
ψ = porosity
ψ_c = filtration percolation threshold

Literature Cited

Adams, D. J., "Chemical Potential of Hard-Sphere Fluids by Monte Carlo Methods," *Mol. Phys.*, **28,** 1241 (1974).

——— "Grand Canonical Ensemble Monte Carlo for a Lennard-Jones Fluid," *Mol. Phys.*, **29,** 307 (1975).

Anderson, J. L., and J. H. Brannon, "Concentration Dependence of the Distribution Coefficient for Macromolecules in Porous Media," *J. Polym. Sci.: Pol. Phys. Ed.*, **19,** 405 (1981).

Brannon, J. H., and J. L. Anderson, "Concentration Effects on Partitioning of Dextrans and Serum Albumin in Porous Glass," *J. Polym. Sci.*, **20,** 857 (1982).

Carnahan, N. F., and K. E. Starling, "Equation of State for Non-Interacting Rigid Spheres," *J. Chem. Phys.*, **51,** 635 (1969).

Casassa, E. F., "Equilibrium Distribution of Flexible Polymer Chains between a Macroscopic Solution Phase and Small Voids," *Polym. Lett., 5, 773 (1967).*

Castro, A., U.S. Patent 4,247,498 (1981); Taken from Kesting (1985).

Chiew, Y. C., and E. D. Glandt, "Percolation Behaviour of Permeable and of Adhesive Spheres," *J. Phys. A,* **16,** 2599 (1983).

——— "Interfacial Surface Area in Dispersions and Porous Media," *J. Colloid Inter. Sci.*, **99,** 86 (1984).

Chiew, Y. C., and G. Stell, "Connectivity and Percolation of Randomly Centered Spheres: Correction to the Percus-Yevick Approximation," *J. Chem. Phys., 90, 4956 (1989).*

Chiew, Y. C., G. Stell, and E. D. Glandt, "Clustering and Percolation in Multicomponent Systems of Randomly Centered and Permeable Spheres," *J. Chem. Phys.*, **83,** 761 (1985).

Davidson, M., U. W. Suter, and W. M. Deen, "Equilibrium Partitioning of Flexible Macromolecules between Bulk Solution and Cylindrical Pores," *Macromol.*, **20,** 1141 (1987).

Fanti, L. A., "Partitioning and Transport in Random Media," PhD Diss., Univ. of Pennsylvania (1989).

Fanti, L. A., and E. D. Glandt, "Partitioning of Spherical Particles into Fibrous Matrices: I. Density Functional Theory," *J. Colloid Inter. Sci.*, in press (1989a).

——— "Partitioning of Spherical Particles into Fibrous Matrices: II. Monte Carlo Simulations," *J. Colloid Inter. Sci.*, in press (1989b).

Giddings, J. C., E. Kucera, C. P. Russel, and M. N. Myers, "Statistical Theory for the Equilibrium Distribution of Rigid Molecules in Inert Porous Networks. Exclusion Chromatography," *J. Phys. Chem.*, **72,** 4397 (1968).

Glandt, E. D., "Density Distribution of Hard-Spherical Molecules inside Small Pores of Various Shapes," *J. Colloid Inter. Sci.*, **77,** 512 (1980).

——— "Distribution Equilibrium between a Bulk Phase and Small Pores," *AIChE J.*, **27,** 51 (1981).

Haan, S. W., and R. Zwanzig, "Series Expansions in a Continuum Percolation Problem," *J. Phys. A,* **10,** 1547 (1977).

Kesting, R. E., *Synthetic Polymeric Membranes,* Wiley, New York (1985).

Kolafa, J., "Autocorrelations and Subseries Averages in Monte Carlo Simulations," *Mol. Phys.*, **59,** 1035 (1986).

Langer, R., and J. Folkman, "Polymers for the Sustained release of Proteins and other Macromolecules," *Nat.*, **263,** 797 (1976).

Limbach, K. W., J. M. Nitsche, and J. Wei, "Partitioning of Nonspherical Molecules between Bulk Solution and Porous Solids," *AIChE J.*, **35,** 42 (1989).

MacElroy, J. M. D., and S.-H. Suh, "Concentration and Non-Continuum Effects in Size-Exclusion Partitioning," *AIChE Symp. Ser.*, **82,** (248) 133 (1986); "Computer Simulation of Moderately Dense Hard-Sphere Fluids and Mixtures in Microcapillaries," *Mol. Phys.*, **60,** 475 (1987).

McMillan, W. G., and J. E. Mayer, "The Statistical Thermodynamics of Multicomponent Systems," *J. Chem. Phys.*, **13,** 276 (1945).

Mitchell, B. D., and W. M. Deen, "Theoretical Effects of Macromolecule Concentration and Charge on Membrane Rejection Coefficients," *J. Membr. Sci.*, **19,** 75 (1984).

Ogston, A. G., "The Spaces in a Uniform Random Suspension of Fibers," *Trans. Farad. Soc.*, **54,** 1754 (1958).

Pike, G. E., and C. H. Seager, "Percolation and Conductivity: A Computer Study: I." *Phys. Rev. B,* **10,** 1421 (1974).

Post, A. J., "Solute Partitioning between a Micropore and a Bulk Solution: A Linear Density Functional Approach," *J. Colloid Inter. Sci.*, **129,** 451 (1989).

Post, A. J., and E. D. Glandt, "Equilibrium Partitioning in Pores with Adsorbing Walls," *J. Colloid Inter. Sci.*, **108,** 31 (1985).

Rikvold, P. A., and G. Stell, "D-Dimensional Interpenetrable-Sphere Models of Random Two-Phase Media: Microstructure and an Application to Chromatography," *J. Colloid Inter. Sci.*, **108,** 158 (1985).

Safran, S. A., I. Webman, and G. S. Grest, "Percolation in Interacting Colloids," *Phys. Rev. A*, **32**, 506 (1985).
Smith, F. G., and W. M. Deen, "Electrostatic Double-Layer Interactions for Spherical Colloids in Cylindrical Pores," *J. Colloid Inter. Sci.*, **78**, 444 (1980); *ibid.*, "Electrostatic Effects on the Partitioning of Spherical Colloids between Dilute Bulk Solution and Cylindrical Pores," **91**, 571 (1983).
Stauffer, D., *Introduction to Percolation Theory*, Taylor & Francis, Philadelphia (1985).
Wiltzius, P., F. S. Bates, S. B. Dierker, and G. D. Wignall, "Structure of Porous Vycor Glass," *Phys. Rev. A*, **36**, 2991 (1987).
Yau, W. W., *Gel Permeation Chromatography*, K. H. Altgelt and L. Segal, eds., Marcel-Decker, New York (1971).
Zhou, Y., and G. Stell, "Fluids inside a Pore—An Intergral-Equation Approach I. General Formalism and Hard Spheres inside Spherical and Slit Pores," *Mol. Phys.*, **66**, 767 (1989a).
——— "Fluids inside a Pore—An Integral-Equation Approach: II. Cylindrical Pores," *Mol. Phys.*, **66**, 791 (1989b).

Manuscript received June 30, 1989, and revision received Sept., 20, 1989.